Width of laminar laboratory rivers

G. Seizilles, O. Devauchelle,* E. Lajeunesse, and F. Métivier
Institut de Physique du Globe de Paris, 1 rue Jussieu, 75238 Paris cedex 05, France
(Received 21 January 2013; published 15 May 2013)

A viscous fluid flowing over plastic grains spontaneously generates single-thread channels. With time, these laminar analogues of alluvial rivers reach a reproducible steady state, showing a well-defined width and cross section. In the absence of sediment transport, their shape conforms with the threshold hypothesis which states that, at equilibrium, the combined effects of gravity and flow-induced stress maintain the bed surface at the threshold of motion. This theory explains how the channel selects its size and slope for a given discharge. In this light, laboratory rivers illustrate the similarity between the avalanche angle of granular materials and Shields's criterion for sediment transport.

DOI: 10.1103/PhysRevE.87.052204 PACS number(s): 45.70.−n, 92.40.Gc, 92.40.Qk, 92.40.qh

I. INTRODUCTION

As alluvial rivers carve their bed in the sediment they carry, they show a beautiful variety of shapes and sizes [1]. The interaction between water flow and sediment transport spontaneously generates a specific morphology and selects a characteristic scale, in a remarkable illustration of morphogenesis [2,3]. When the sediment discharge increases, rivers typically develop a network of closely intertwined threads to produce a braided pattern [4–6]. Conversely, at moderate transport rates, alluvial rivers exhibit a well-defined channel over distances much longer than their width. The morphology of single-thread rivers obeys empirical scaling laws [7,8] such as Lacey's equation [9], which states that the width of a river is proportional to the square root of its discharge. This universal behavior suggests a common physical origin [10], yet there is no consensus about what this origin is.

A simple way to explain Lacey's law is to assume that the river bed is at the threshold of sediment transport [11–13]. According to this theory, the sum of gravity and fluid friction maintains the sediment exactly at the threshold of motion, everywhere across the river bed. For a given discharge, this mechanism sets the width and the streamwise slope of a channel. Despite its simplicity, this theory accords well with field data [14–16], at least in order of magnitude. However, it is often considered incomplete, as it cannot account for sediment transport [17] while most alluvial rivers are active. In addition, the threshold theory neglects many aspects of natural streams, such as bank cohesion and vegetation, sediment heterogeneity, or variations of the water discharge. It is therefore delicate to discriminate between theories on the basis of field measurements only [18,19].

Laboratory flumes imitate natural rivers, while vastly reducing the number of parameters susceptible to influence their shape [20,21]. This relative simplicity facilitates the physical interpretation of experimental observations. As long as the experimental setup preserves the essential processes, laboratory experiments can greatly help us to understand natural rivers.

Most laboratory flumes form braids [22,23], probably due to the growth of unstable bedforms [24]. To maintain a single channel, Ikeda halved his flume with a solid wall [25]. Here, we combine a viscous fluid with low-density sediment grains to increase the saturation length of sediment transport, and thus stabilize the bed [26,27]. As a result, our experimental setup spontaneously generates stable single-thread channels. We use these channels to evaluate the threshold hypothesis.

II. LABORATORY RIVERS

The experimental setup consists of an inclined plane (190 × 90 cm) covered with an initially flat layer of plastic sediment (Fig. 1). We use plastic grains (density $\rho_s \approx 1520 \pm 50\ \mathrm{g\,L^{-1}}$, grain diameter $d_s \approx 220 \pm 80\ \mu\mathrm{m}$) to reduce their density, and thus increase the typical distance a grain travels over when transported by the flow. The grains are irregularly shaped. At the outlet, the sediment layer is held by a 25-mm-high slat, over which water runs before leaving the experiment. The sediment layer is always thicker than the river depth.

An experiment begins when water is allowed to flow over the sediment bed at a constant discharge. To increase the viscosity of the fluid, we mix glucose and water (about 50% in weight, viscosity $\nu \approx 15 \times 10^{-6} \pm 5 \times 10^{-6}\ \mathrm{m\,s^{-2}}$, density $\rho_f \approx 1220 \pm 30\ \mathrm{g\,L^{-1}}$). This maintains the Reynolds number at a low value and guarantees that the flow remains laminar (Re ≈ 20–50, calculated with the flow depth). Additionally, a high viscosity further increases the sediment travel distance.

During the first minutes of an experiment, the flow spreads over the entire sediment surface, forming a uniform sheet of water. After a few tens of minutes, a favored flow path appears near the center of the experiment. As sediment is further removed from this higher-flow area, a channel becomes apparent. Around it, the sediment surface emerges from the flow.

During the next day or two, the channel gets narrower and deeper, as it transports less and less sediment, until it reaches its equilibrium state (no visible moving grains). At equilibrium, a channel is a few centimeters wide, depending on the fluid discharge. In most experimental runs, the channel is a single straight thread, although some rivers show a weak sinuosity and multiple threads near the outlet.

The channel planform is typically smooth, with a well-defined width (Fig. 1). The inlet deforms the channel morphology over 5 to 20 cm, a distance much larger than the expected saturation length for sediment transport (about the

*devauchelle@ipgp.fr

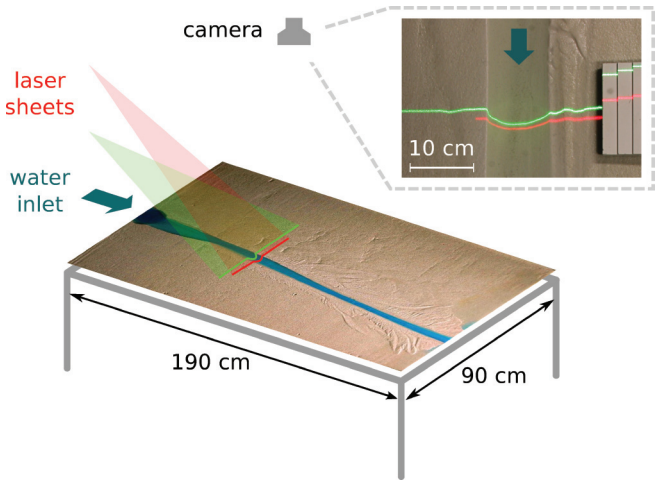

FIG. 1. (Color online) Schematic view of the experimental setup. Inset: top view of a laminar river, with the two laser sheets used to measure the cross section.

grain size in a viscous flow [28]). The influence of the outlet extends upstream over a comparable distance.

The equilibrium state of the channel does not depend significantly on the initial conditions. Imperfections of the sediment layer do not seem to force the final position of the stream, nor does an initially fabricated channel. If the plane is steeper than the equilibrium slope, the channel incises the sediment layer in the neighborhood of the water inlet and deposits sediment near the outlet, creating a small alluvial fan. If, conversely, the initial slope is too low, the channel reaches its equilibrium slope with the inverse configuration. In both cases, the time to equilibrium increases. We therefore start each experiment as close to the equilibrium slope as possible, by trial and error.

Once the channel has reached equilibrium, we measure its cross section with two laser sheets at different incidence angles (Fig. 1). This technique yields both the sediment bed elevation and the position of the water surface [29]. Most channels have a regular and symmetrical cross section (Fig. 2), perturbed only by low-amplitude bedforms or miniature terraces created by the lateral displacement and the narrowing of the channel. In some cases, the river has created small levees in the deposition zone.

Overall, the experiments are very reproducible. The channel width is chiefly controlled by the water discharge and it varies by less than 30% along the river (except near the plane limits).

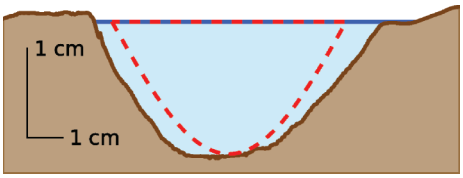

FIG. 2. (Color online) Example of a laminar river cross section at equilibrium. The brown (below) and blue (above) lines show the sediment bed elevation and the average position of the water surface, respectively. The discharge is $Q_w = 1.1$ L min^{-1}. The dashed red line shows the theoretical cross section [Eqs. (9) and (13)].

III. RIVERS AT THRESHOLD

Our experimental rivers slowly evolve towards a stationary shape, which does not depend significantly on the initial conditions. This behavior suggests that, at the end of an experiment, the channel has reached a mechanical equilibrium. We suggest that this equilibrium corresponds to the theory first proposed by Glover and Florey [11], namely, that the river bed is at threshold for sediment transport.

In this section, we rederive the threshold theory from basic principles in order to (i) adapt it to laminar flows and (ii) relate the Shields parameter, which defines the threshold for sediment transport, to the avalanche angle of granular materials.

A. Avalanche angle and Shields parameter

The conical shape of a heap of dry sand is determined, at first order, by the avalanche angle of the sand. This angle materializes the equilibrium of a grain lying at the surface of the heap and submitted to gravity. The tangential force $\mathbf{f}_t$ tends to dislodge the grain, whereas the normal force $\mathbf{f}_n$ holds the grain in place. The maximum slope a heap can sustain defines the Coulomb friction coefficient μ as

$$\mu = \frac{\|\mathbf{f}_t\|}{\|\mathbf{f}_n\|} = \tan\phi_r, \tag{1}$$

where ϕ_r is the avalanche angle. The slope of a slowly built heap of our sediment corresponds to a friction coefficient of $\mu \approx 0.7$, a typical value for a noncohesive granular material.

When a flow applies a force on a grain, the same reasoning holds. A fluid flowing above a horizontal layer of sediments applies a tangential force to each grain, of norm

$$\|\mathbf{f}_t\| = \alpha d_s^2 \tau, \tag{2}$$

where d_s, τ, and α are the grain diameter, the shear stress applied by the flow, and a coefficient of order one, respectively. The coefficient α depends on the grain's shape and on the Reynolds number of the flow around it. At low grain Reynolds number [$\mathrm{Re}_s = d_s^2\,\tau/(\rho_f\,\nu^2)$], we expect no vertical force on the grain other than weight and buoyancy. The normal force thus reads

$$\|\mathbf{f}_n\| = \beta(\rho_s - \rho_f) g d_s^3, \tag{3}$$

where g and β are the acceleration of gravity and a shape factor of order one, respectively. At the threshold of motion, the ratio of tangential and normal forces equals the critical friction coefficient. This relationship is usually expressed with the Shields parameter and its threshold value θ_t [30]:

$$\frac{\tau}{(\rho_s - \rho_f) g d_s} = \frac{\beta}{\alpha}\mu \equiv \theta_t. \tag{4}$$

The threshold Shields parameter depends weakly on the grain Reynolds at the grain scale, with typical values between 0.01 (turbulent flow) and 0.3 (viscous flow [31]). We have measured the threshold of motion for our plastic sediment in an independent 3-cm-wide, hard-walled channel. At a grain Reynolds number of $\mathrm{Re}_s \approx 0.03$, we find $\theta_t \approx 0.25$.

Equation (4) illustrates the fundamental equivalence between the threshold for sediment transport and the onset of avalanches in dry granular materials [32]. This equivalence manifests itself in the geometry of laminar rivers.

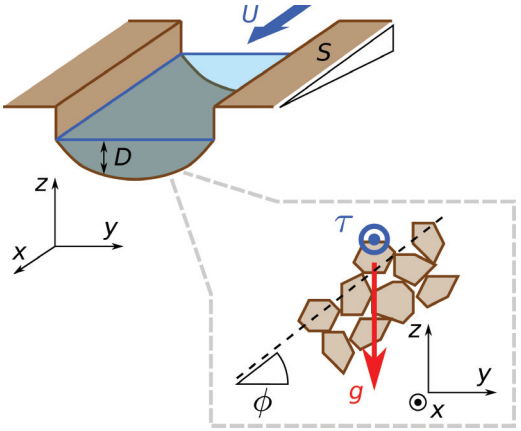

FIG. 3. (Color online) Schematic representation of a laboratory river. Both the depth D and the velocity U are functions of the transverse coordinate y. The river is invariant in the streamwise direction x.

B. Equilibrium theory

As long as we consider a horizontal layer of sediments, the shape factors α and β may seem artificial since experiments yield directly the critical Shields parameter (although Shields himself introduces shape factors [30]). However, the configuration of alluvial rivers requires that we explicitly distinguish between the effect of gravity and the effect of the flow.

We consider a straight laminar river, which has carved its bed in a layer of uniform sediment (Fig. 3). We further assume that the equilibrium channel is such that, everywhere across the bed, sediment grains are at the threshold of motion. Noting that gravity and the flow-induced stress are orthogonal components of the tangential force, the threshold condition reads

$$\left[\frac{\alpha\tau}{\beta(\rho_s-\rho_f)gd_s}\right]^2+\sin^2\phi=\mu^2\cos^2\phi, \tag{5}$$

where ϕ is the angle of the bed with respect to the horizontal, in the transverse direction. We have neglected the longitudinal slope of the river in the expression of the grain weight (the effect of slope is embedded in the fluid friction only). In our experiments, the resulting error is less than 1%.

The shear stress τ results from the flow which, in turn, depends on the river's shape. Equation (5) thus defines a free-boundary problem—the channel cross section must be such that the flow satisfies it. At low Reynolds number, the flow in a straight channel is laminar and satisfies a two-dimensional Poisson equation in the transverse plane (y,z). However, the exact two-dimensional free-boundary problem is not solvable analytically and proves numerically challenging. For the sake of simplicity, we assume that the channel is flat enough to use the shallow-water approximation (that is, we neglect the cross-stream transfer of momentum). Consequently, the fluid friction on the river bed balances gravity:

$$\tau=\rho_f gSD, \tag{6}$$

where S is the longitudinal slope of the channel. In accordance with the shallow-water approximation, the transverse slope is moderate ($\cos\phi\approx 1$) and Eq. (5) becomes a first-order differential equation,

$$\left(\frac{SD}{L}\right)^2+\left(\frac{\partial D}{\partial y}\right)^2=\mu^2, \tag{7}$$

where we define the characteristic length

$$L=\frac{\theta_t(\rho_s-\rho_f)d_s}{\mu\rho_f}, \tag{8}$$

based on Eq. (4). This length, which depends on the sediment only, is of the order of the grain size (except for almost buoyant materials). After Eq. (7), the typical scale of the channel is L/S. A small slope thus induces a clear separation between the grain scale and the channel size.

A solution to the differential equation (7) is

$$D=\frac{\mu L}{S}\cos\left(\frac{Sy}{L}\right). \tag{9}$$

The cross section of our laboratory channels resembles a cosine (Fig. 2). More specifically, the theory predicts an aspect ratio of $\pi^2/(2\mu)\approx 7.0$ (width over average depth), regardless of the water discharge. Despite considerable scatter in the data, our experiments reasonably conform to this prediction (Fig. 4).

According to Eq. (9), the banks are at the angle of repose. This remark holds beyond the shallow-water approximation since the fluid friction vanishes at the bank.

As illustrated by Eq. (7), a river at threshold embodies the two end members of a grain equilibrium: the force balance introduced by Shields at the center of the channel ($\partial D/\partial y=0$) and Coulomb's equilibrium at the banks ($D=0$).

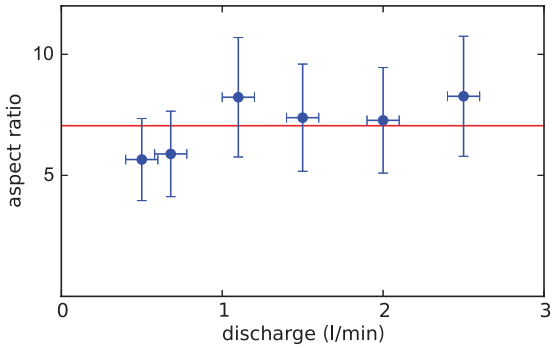

FIG. 4. (Color online) Aspect ratio of laminar laboratory rivers at equilibrium, as a function of the water discharge (blue dots). The red line corresponds to the theoretical aspect ratio $\pi^2/(2\mu)\approx 7.0$. Each data point is the average of two or three cross sections measured on the same river (for the fifth run only, width and depth were measured with a ruler). The width varies by less than 30% along the river (vertical error bars). During an experiment, the water discharge varies by less than 0.1 ℓ min^{-1} (horizontal error bars).

C. Scaling laws for laminar rivers

So far, the threshold hypothesis predicts the river's shape, but not its size. Indeed, the scale of the cosine channel represented by Eq. (9) depends on the river slope S. To go further, we need to consider the mass and momentum balances for the fluid.

According to the shallow-water approximation (also referred to as the "lubrication approximation" for viscous flows),

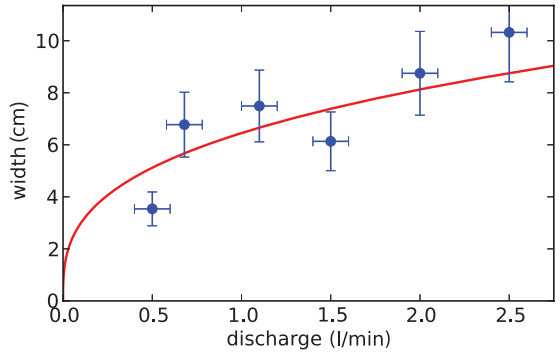

FIG. 5. (Color online) Width of laboratory rivers as a function of discharge (blue dots). The red line corresponds to the threshold theory, without any fitted parameter [Eq. (13)]. Each data point is the average of two or three cross sections measured on the same river (for the fifth run only, width and depth were measured with a ruler). The width varies by less than 30% along the river (vertical error bars). During an experiment, the water discharge varies by less than $0.1\,\ell\ \mathrm{min}^{-1}$ (horizontal error bars).

the fluid friction at the bottom of the channel balances gravity. The resulting Poiseuille flow satisfies

$$\frac{3\nu U}{D} = gSD, \tag{10}$$

where U is the vertically averaged water velocity. Finally, the discharge reads

$$Q_w = \int_{\text{channel}} U D dy. \tag{11}$$

In combination with the momentum balance (10) and the threshold cross section (9), the water mass balance yields two scaling laws:

$$S = \left[\frac{\theta_t(\rho_s - \rho_f)d_s}{\rho_f}\right]^{4/3}\left(\frac{4g}{9\mu\nu Q_w}\right)^{1/3}, \tag{12}$$

$$W = \frac{\pi L}{S} = \frac{\pi}{\mu^{2/3}}\left[\frac{9\nu\rho_f Q_w}{4g\theta_t(\rho_s - \rho_f)d_s}\right]^{1/3}. \tag{13}$$

Equation (13) is the equivalent of Lacey's law for a laminar river, where the cubic root of the water discharge takes the place of the classical square-root dependence.

Our experimental data gather around this prediction (Fig. 5). Its significant dispersion results from the actual variability of the river width, rather than from measurement uncertainties. Indeed, the widest cross section of a river can be 30% wider than the narrowest one, whereas the measurement uncertainty is of the order of the capillary length only (a few millimeters).

With our experimental setup, discharges smaller than $0.5\,\ell\ \mathrm{min}^{-1}$ or larger than $2.5\,\ell\ \mathrm{min}^{-1}$ are impracticable. As a consequence, the data do not constrain strongly the exponent of the width-discharge relation. However, the threshold theory correctly predicts both its order of magnitude and its trend, without any fitted parameter. We thus believe that the balance between shear stress and fluid friction embodied by Eq. (7) sets the size of our laboratory rivers.

Assuming this is correct, we use Eqs. (8) and (12) to rescale the measured cross section according to the water discharge. Doing so for each run, we then compute the mean cross section for all of our experiments (Fig. 6). The resulting shape resembles a cosine, with a more rounded base. This slight disagreement might result from the flow two-dimensionality, which we have neglected in order to derive the cosine cross section.

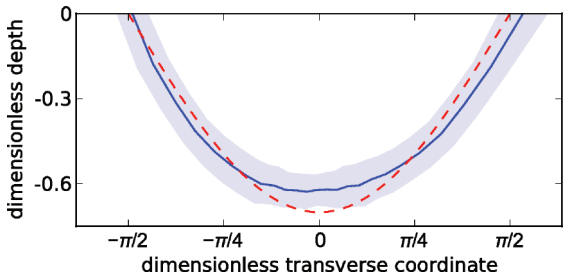

FIG. 6. (Color online) Average cross section of laboratory rivers (blue solid line). For each water discharge, the cross section is rescaled with L/S [Eqs. (8) and (12)]. The average is computed in polar coordinates relative to the center of the cross section. The shaded area indicates the variance of the cross-sections sample. Red dashed line: cosine cross section predicted by Eq. (9).

According to Eq. (12), the discharge of a river not only sets its size, but also imposes its slope. Unfortunately, assessing this prediction experimentally is difficult. In our experiments, we expect a slope of about 10^{-3}; over the entire river, this corresponds to a change of about a millimeter in bed elevation. We have not reached this accuracy, despite an attempt with a moiré technique [33]. However, before each experiment, we set the slope of the initial flat bed close to its theoretical value. If the initial bed is too steep, the river incises deeply into the sediment layer near the water inlet. Conversely, too small a slope generates an alluvial fan near the inlet, indicating deposition. These observations suggest that the river tends towards an equilibrium slope.

IV. DISCUSSION AND CONCLUSION

The characteristic size and shape of laminar laboratory channels accord closely with the threshold theory of alluvial rivers. This need not have been the case, for two reasons at least. First, the shallow-water hypothesis is a rather severe approximation, especially since we expect the slope to reach the avalanche angle at the bank. Second, the cosine solution to the equilibrium equation (7) is not unique. Indeed, as Henderson pointed out, a flat section at threshold enclosed with two half cosines is also a solution [12]. To understand why the narrowest solution is selected, we need to consider the path towards equilibrium. To take this history into account, we must add sediment transport to the theory.

The threshold theory has been compared with reasonable success to field data [14,15], suggesting that the force balance which it is based on sets the shape of alluvial streams. However, the aspect ratio of most rivers is significantly larger than the theoretical value. Since alluvial rivers generally transport a nonvanishing load of sediments, the threshold theory appears as a limit case that explains the orders of magnitudes, but still lacks an ingredient.

Assuming that the bed is slightly above threshold in the framework proposed here leads to a paradox: moving particles

would be pulled towards the middle of the channel by gravity, thus preventing equilibrium [17]. Various mechanisms have been invoked to compensate for gravity: suspended particle diffusion [34], diffusion of lateral momentum [17], or riparian vegetation [35]. None of them, though, applies to laminar laboratory rivers and the stable channel paradox remains a stimulating question for future investigations.

ACKNOWLEDGMENTS

We are grateful to A. Limare, H. Bouquerel, Y. Gamblin, T. Rivet, and A. Vieira for building the experimental setup and developing the measurement methods. We also thank P. Y. Lagrée and Y. Klinger for stimulating suggestions. O.D. would like to thank A. P. Petroff, H. Seybold, and D. H. Rothman for fruitful discussions.

[1] M. Church, Annu. Rev. Earth Planet Sci. **34**, 325 (2006).
[2] M. Cross and H. Greenside, *Pattern Formation and Dynamics in Nonequilibrium Systems* (Cambridge University Press, New York, 2009).
[3] J. P. Gollub and J. S. Langer, Rev. Mod. Phys. **71**, 396 (1999).
[4] J. H. Mackin, Geol. Soc. Am. Bull. **59**, 463 (1948).
[5] S. A. Schumm, M. P. Mosley, and W. E. Weaver, *Experimental Fluvial Geomorphology* (Wiley, New York, 1987), p. 413.
[6] F. Métivier and L. Barrier, *Gravel Bed Rivers: Processes, Tools, Environments*, edited by M. Church, P. Biron, and A. Roy, Chap. 34 (Wiley, 2012), pp. 474–501.
[7] L. B. Leopold and T. Maddock, *The Hydraulic Geometry of Stream Channels and Some Physiographic Implications*, Vol. 252 (US GPO, Washington, DC, 1953).
[8] G. Parker, P. R. Wilcock, C. Paola, W. E. Dietrich, and J. Pitlick, J. Geophys. Res.: Earth Surface **112**(F4), 1 (2007).
[9] G. Lacey, Minutes Proc. Inst. Civ. Eng. **229**, 259 (1930).
[10] C. Paola and M. Leeder, Nature (London) **469**, 38 (2011).
[11] R. E. Glover and Q. L. Florey, Laboratory Report No. Hyd-325, United States Department of the Interior, Bureau of Reclamation (Denver, Colorado, 1951), p. 44.
[12] F. M. Henderson, J. Hydraul. Div. ASCE **87**, 109 (1961).
[13] H Savenije, J. Hydrol. **276**, 176 (2003).
[14] E. D. Andrews, Bull. Geol. Soc. Am. **95**, 371 (1984).
[15] O. Devauchelle, A. P. Petroff, A. E. Lobkovsky, and D. H. Rothman, J. Fluid Mech. **667**, 38 (2011).
[16] A. P. Petroff, O. Devauchelle, A. Kudrolli, and D. H. Rothman, Comptes Rendus Geosci. **344**, 33 (2012).
[17] G. Parker, J. Fluid Mech. **89**, 127 (1978).
[18] M. S. Yalin and A. M. F. da Silva, *Fluvial Processes* (International Association of Hydraulic Engineering and Research, Delft, 2001).
[19] R. G. Millar, Geomorphology **64**, 207 (2005).
[20] L. Malverti, E. Lajeunesse, and F. Métivier, J. Geophys. Res. **113**, F04004 (2008).
[21] E. Lajeunesse, L. Malverti, P. Lancien, L. Armstrong, F. Métivier, S. Coleman, C. E. Smith, T. Davies, A. Cantelli, and G. Parker, Sedimentology **57**, 1 (2010).
[22] L.B. Leopold and M. G. Wolman, *River Channel Patterns: Braided, Meandering, and Straight* (US GPO, Washington, DC, 1957).
[23] B. Federici and C. Paola, Water Resour. Res. **39**, 1162 (2003).
[24] O. Devauchelle, C. Josserand, P. Y. Lagrée, and S. Zaleski, Phys. Rev. E **76**, 056318 (2007).
[25] S. Ikeda, J. Hydraul. Eng. **107**, 389 (1981).
[26] F. Charru, Phys. Fluids **18**, 121508 (2006).
[27] O. Devauchelle, L. Malverti, E. Lajeunesse, P. Y. Lagrée, C. Josserand, and K. D. N. Thu-Lam, J. Fluid Mech. **642**, 329 (2010).
[28] F. Charru, H. Mouilleron, and O. Eiff, J. Fluid Mech. **519**, 55 (2004).
[29] A. Fourrière, Ph.D. thesis, Université Paris Diderot, 2009.
[30] A. Shields, Application of Similarity Principles and Turbulence Research to Bed-load Movement. Hydrodynamics Laboratory Publication 167. US Department of Agriculture, Soil Conservation Service Cooperation Laboratory, California Institute of Technology, Pasadena, California, 1936.
[31] A. E. Lobkovsky, A. V. Orpe, R. Molloy, A. Kudrolli, and D. H. Rothman, J. Fluid Mech. **605**, 47 (2008).
[32] T. Loiseleux, P. Gondret, M. Rabaud, and D. Doppler, Phys. Fluids **17**, 103304 (2005).
[33] A. Limare, M. Tal, MD Reitz, E. Lajeunesse, and F. Métivier, Solid Earth Discuss. **3**, 187 (2011).
[34] G. Parker, J. Fluid Mech. **89**, 109 (1978).
[35] M. Tal and C. Paola, Geology **35**, 347 (2007).